The SALT HRS spectrograph: final design, instrument capabilities and operational modes

D. G. Bramall[a], R. Sharples[a], L. Tyas[a], J. Schmoll[a], P. Clark[a], P. Luke[a], N. Looker[a], N. A. Dipper[a], S. Ryan[b], D. A. H. Buckley[c], J. Brink[c], S. I. Barnes[d]
[a] Centre for Advanced Instrumentation, Durham University, U.K.;
[b] School of Physics, Astronomy and Mathematics, University of Hertfordshire, U.K.;
[c] Southern African Large Telescope, South African Astronomical Observatory, South Africa;
[d] Department of Physics and Astronomy, University of Canterbury, New Zealand.

ABSTRACT

The high-resolution échelle spectrograph, SALT HRS, is at an advanced stage of construction and will shortly become available to the user community of the Southern African Large Telescope (SALT). This paper presents a commentary on the construction progress to date and gives the instrument's final specification with refined estimates for its performance based on the initial testing of the optics and the science-grade detectors. It also contributes a discussion of how the fibre input optics have been tailored to specific scientific aspirations to give four distinct operational modes. Finally, the use of the instrument is discussed in the context of the most common science cases.

Keywords: Spectrograph, échelle, SALT

1. INTRODUCTION

SALT HRS will be the third and final first-light instrument on SALT, the largest optical telescope in the southern hemisphere. It was proposed as a high efficiency, fibre-fed, single object spectrograph to accomplish a varied range of astronomical science. It is principally suited to science that requires essentially complete optical spectra at high spectral resolution, of targets with a low areal density on the sky. The optical configuration of the spectrograph was originally developed at the University of Canterbury's Department of Physics and Astronomy. The design was then handed over to the University of Durham's Centre for Advanced Instrumentation for manufacture where work has been undertaken to complete the residual mechanical and electronic design and to tailor the feed optics to maximise the instrument's science capability. Manufacturing is now well underway and a completion date of early 2011 is foreseen.

1.1 Primary Instrument Specifications

SALT HRS will deliver:

- stable, high-resolution spectra at resolutions of R ~ 16000, 37000 and 67000
- simultaneous capture of object and sky samples (for good background subtraction)
- wide wavelength coverage ($\Delta\lambda$ ~ 500 nm) with
    - a short wavelength limit down to 380 nm, i.e. shortward of the Ca II 393, 396 nm lines and
    - a long wavelength limit at 890 nm, i.e. longward of the 850-865 nm Ca IR triplet
- wavelength stability commensurate with achieving a few ms^{-1} accuracy in radial velocities

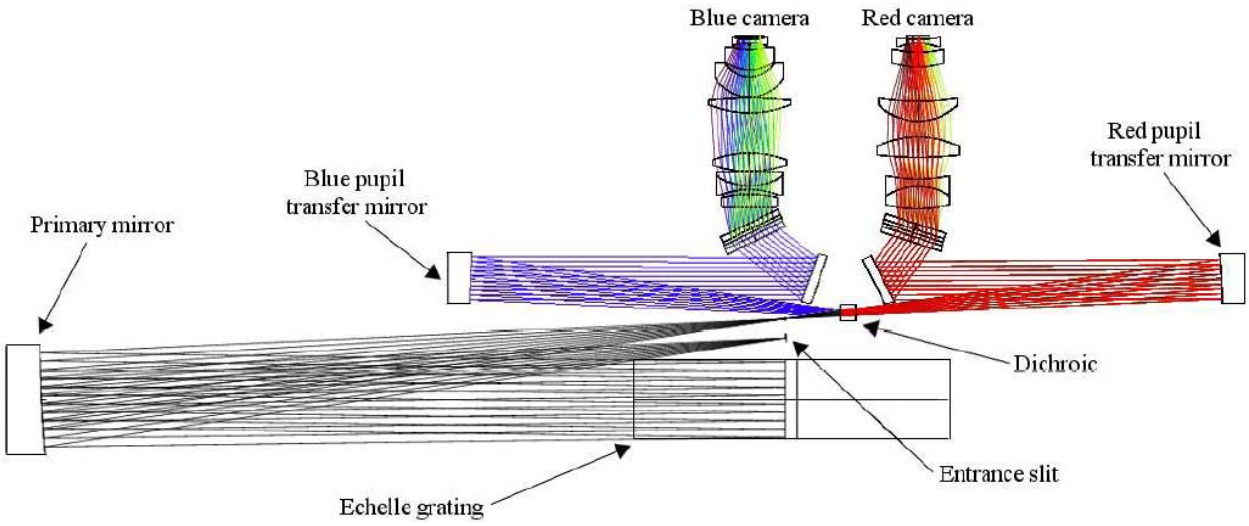

Figure 1. Schematic of the optical layout of the main spectrograph (input optics not shown). Reprinted from Barnes *et al*[1].

2. THE FINALISED OPTICAL DESIGN

2.1 Spectrograph Design

The spectrograph is a white pupil design that employs a 214mm x 800mm R4 échelle grating which is illuminated by a 200mm diameter beam. The grating has a nominal blaze angle of 76˚. The dispersed light is split into separate blue (370nm to 555nm) and red (555nm to 890nm) arms by a dichroic beam splitter. Cross dispersion is achieved by way of two volume phase holographic gratings (VPHGs) that are positioned in front of the two fully dioptric cameras. The spectrograph's operation is described in some detail in a previous paper[1], so here we restrict ourselves to discussing some of the important trade-offs that were made during the procurement phase. An overview of the optical design is, however, given in Figure 1.

2.1.1 The Échelle Grating: monolithic grating *vs.* mechanically-aligned mosaic

The manufacture of such large, monolithic échelle gratings is not trivial[2] and during the procurement phase the option of mechanically aligning two smaller gratings was explored as an alternative to having a grating with two sub-masters replicated on a single substrate. Much of the literature on aligning smaller individual gratings is for the purposes of chirped laser amplification. The reported results show that it is relatively easy to measure grating alignment interferometrically and de-convolve the interferograms into corrective adjustments in five degrees of freedom, namely yaw, pitch, roll, piston and groove-perpendicular offset. Zemax simulations were done to explore the consequences of angular misalignments. Piston and groove perpendicular offset were found to only require low accuracy alignment as the grating is used in a regime well below the diffraction limited resolving power. The image was found to be most sensitive to yaw error where large errors would impair the slit image. Starting with the grating in rough alignment (better than 1 arcminute), the yaw error could be removed first by co-aligning the beams of an order near the blaze wavelength of the grating. It would then be possible to cancel out small residual yaw, roll and pitch errors in the arcsecond regime by observing the profile of the spectral line and tipping and tilting the grating.

It was found that, mechanically, the required relative motions and positioning accuracies could be achieved in a cost-effective manner using piezo actuators. However, the long term stability of the mechanical alignment (and hence the usefulness of such a grating for radial velocity science) *could possibly* be compromised. Because of the time required to undertake further research, and with the support of Richardson Gratings, a brand of Newport Corporation, the option of a monolithic grating was in the end pursued for SALT HRS.

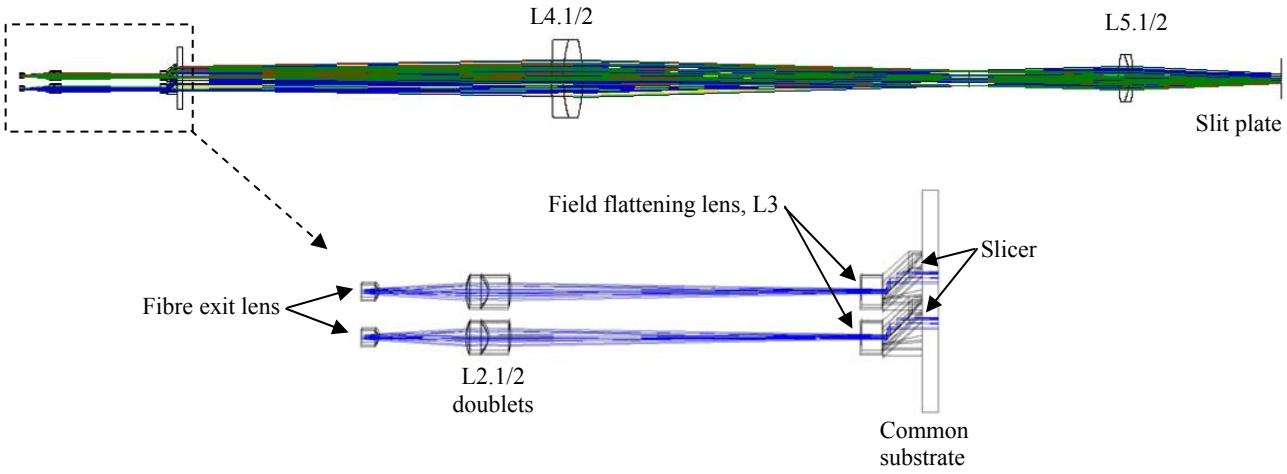

Figure 2. Fore optics for one sliced mode (object and sky fibres shown).

2.1.2 Spectral Formats: reduction in extreme red limit *vs.* loss of light at crossover

Another issue that arose during the procurement phase was the crossover performance of the dichroic. The dichroic coating has a 20nm wide transition region either side of the nominal 50% transmission wavelength (located at 555nm) where some fraction of light is reflected and the remainder transmitted (see Figure 3). Light at these transition wavelengths will be transmitted to the focal plane of *both* CCDs resulting in unintentional orders which overshoot the CCDs (albeit with diminishing intensity). The instrument's opto-mechanical design provides the capability to move the position of spectra on the CCD by tilting the VPHG gratings, so it was considered whether the instrument should be set up to have complete coverage or sacrifice the extreme red orders. When the spectral formats for the two cases were computed, it was felt that the science case was more strongly in favour of accepting a dip in throughput at the crossover region in favour of capturing red wavelengths out to 890nm to make sure the continuum longward of the near-IR Ca II triplet is well measured.

2.1.3 VPHG tuning: throughput peak at extreme blue *vs.* mid-band

It is possible to modify the design parameters of the VPHG cross-dispersers to tune the peak of the S-P plane averaged first order efficiency of the grating. Shifting the peak efficiency of the blue grating would ostensibly provide compensation for the absorption losses inherent in the optical fibres at shorter wavelengths, leading to a flatter overall

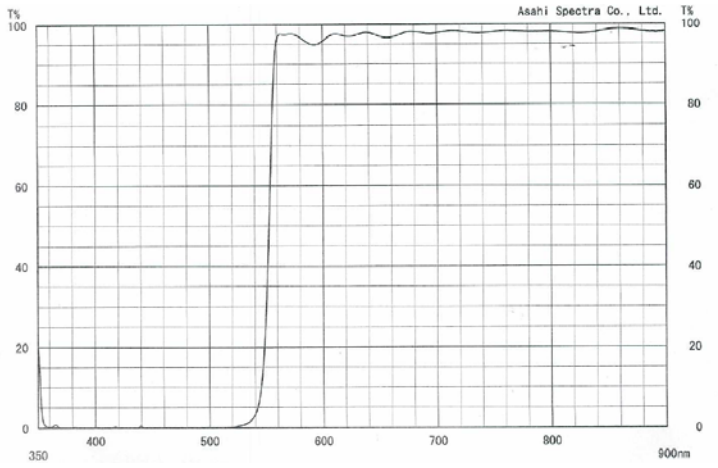

Figure 3. Measured dichroic crossover performance. (Courtesy of Asahi Spectra Co., Ltd.)

instrument throughput efficiency. In practice however, the VPHG first order efficiency predictions (computed using rigorous coupled-wave analysis techniques and accounting for scatter, absorption, losses to higher orders and Fresnel reflections) show that to shift the average s-plane and p-plane efficiency peak to 390nm (10% overall gain at this wavelength), results in a reduction in maximum efficiency from ~91% to ~88% and throughput reduced by approximately 7% between 540nm and 530nm, which is quite a severe penalty. Furthermore it would also require a change to the incidence angle of the grating – an alteration that was not trivial to implement due to the proximity of the VPHGs and cameras. In consultation with the SALT Science Working Group, a decision was therefore made to keep the VPHG optimised to 450nm. The instrument throughput predictions are given in Section 2.4.2.

2.2 Fibre Feed and Input Fore Optics

There are three image-sliced modes plus a further, unsliced, low resolution mode having direct fibre injection. The low resolution mode (R ~ 16000) is uniquely capable of operating in a "nod-and-shuffle"[3] manner for improved accuracy in the subtraction of the sky background. The medium and high resolution modes, using 600μm and 350 μm core-diameter fibres, have Bowen/Walraven-type slicers and offer resolutions of R ~ 37000 and R ~ 67000 respectively. The final sliced mode also has 350 μm core-diameter fibres but features additional double scramblers to improve long-term spectral stability and an (optional) iodine cell, and is primarily targeted at radial velocity science. This mode was implemented at R ~ 67000, because of the importance of adequately sampling the line profiles in order to achieve sub-resolution element accuracy. (An error of 0.5 ms^{-1} corresponds to 10^{-4} of a resolution element.) All four modes are capable of capturing object and sky spectra simultaneously. All the feed optics (with the exception of the iodine cell and fibre double scrambler) have been moved inside the vacuum vessel to take advantage of the immunity from external temperature fluctuations and atmospheric pressure variations.

The fore optics, duplicated for all three of the image sliced modes, are shown for both object and sky fibres in Figure 2. They transform the f/3.8 fibre exit focal ratio to f/25 (as required by the slicers) by way of a doublet and perform field flattening. The image formed within the slicers is then matched to the collimator by two further cemented doublets that are common to all sliced modes. A mask is positioned near the focus point at the slit plate that allows light from only the selected resolution mode to pass through. A fast shutter interrupting all beams is also included at this location. The total length of the fore optics from fibre surface to slit plate is 803.1 mm. The low resolution mode fibres are unsliced and are fed into the spectrograph via a pair of fold mirrors located in front of the slit plate to avoid vignetting caused by the fibre exit lenses.

2.2.1 Optical Fibre Performance Testing

As the instrument is fibre fed, work is ongoing to quantify the effect of focal ratio degradation (FRD) including a simulation of the effect of SALT's variable pupil illumination. The main consequence of FRD is overfilling of the collimator and hence loss in throughput. The test set-up was adapted from Schmoll[4]; the light feeding the fibre under test was collimated, filtered (to give a defined spectral passband), passed through a variable aperture stop (which controls the effective input focal ratio of the fibre) and finally focussed on the fibre end. A pentaprism was temporarily inserted into the collimated beam to assist in aligning the system. The output end of the fibre was immersion coupled to the CCD window.

Results were obtained for two fibre samples (Polymicro FBP400 and FBP600), the closest available to the 350 μm custom drawn and 500μm core fibre that will be used in SALT HRS. Each fibre was tested with input focal ratios from f/2.8 (the maximum size the lenses would allow for), f/3.85 (corresponding exactly to the SALT HRS feed), f/5 and f/8 with wavelengths ranging from 440nm to 830nm. In the case of the 400μm core diameter fibre we have found in excess of 95.7% throughput. Throughput did not change significantly between f/2.8 and f/5 although a more significant drop in performance was seen with this fibre at f/8. Throughput was also fairly constant between 830nm to 532nm, but the 440nm measurements showed a ~4% drop. A hexagonal shaped mask was also used to interrupt a 532nm input beam to simulate the effect of the SALT moving pupil. It was found that the profile of the input beam imparts a measurable effect on the FRD only where the beam occlusion is extreme. At the spectrograph's f/3.85 input, the FRD response is broadly flat until the pupil is reduced to ~16% of maximum. In operation, the SALT collecting area typically only varies between $38m^2$ - $55m^2$ so any effect should be minor.

2.3 Calibrations and Ancillary Equipment

The principal method of generating the calibration frames for data reduction will be to feed the spectrograph from the telescope's own calibration light source. A module within the telescope's spherical aberration corrector (SAC) provides

uniform focal plane illumination by thorium-argon and smooth-spectrum sources. This module duplicates the far-field illumination pattern for arbitrary telescope exposure tracks. Where the nod and shuffle mode is to be used during the night's observations, separate calibration frames will need to be taken with the charge being shuffled on the CCD.

For monitoring the long term instrument drift (specifically, PSF stability and throughput stability) SALT HRS will be equipped with an additional 100µm fibre input fed from the same lamp as the simultaneous ThAr injection. The small core size of this fibre implies that the filling efficiency will be low, however the resulting long exposures are not a major inconvenience as these checks will be mainly scheduled during the daytime where ~20 s exposures are deemed acceptable.

An exposure meter has been designed to make use of the light incident on the 16mm gap between the two replicated gratings that would otherwise be lost. Light is focused onto an optical fibre light guide by a strip mirror and guided onto the active area of a Hamamatsu H7421-50 photomultiplier tube (which has a QE of 12% at 800nm) and is located outside the instrument's vacuum chamber. A photomultiplier tube was chosen because the currently available avalanche photodiode type detectors cannot deliver the low dark counts required in combination with the (relatively) large collecting area necessary when feeding them via a fibre light guide. The low efficiency of the system is justified because the Doppler velocity calculations which require the flux-weighted exposure mid-point (that the exposure meter data provides) are normally only done on bright stars.

2.4 Expected Performance

2.4.1 Image Quality

The design of the input optics, the aforementioned design trade-offs and the re-optimisation of the cameras with known glass melt data have all been made with the goal of not degrading the image quality from the original spectrograph design. Spot diagrams showing image quality at the middle and ends of three example orders are shown in Figure 4. Best

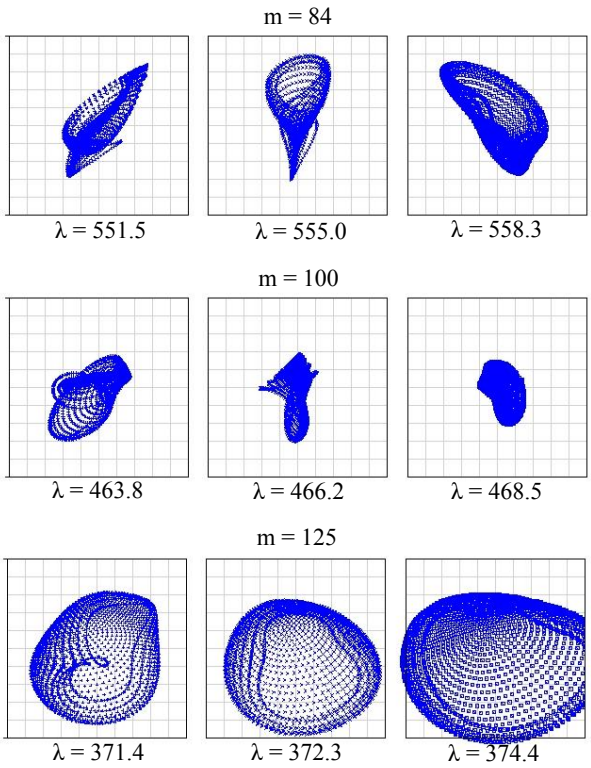

Figure 4. The image quality of the blue arm. Spot diagrams are shown for the middle and ends of orders. Wavelengths and order numbers are noted. Each box is three pixels (45 µm) square.

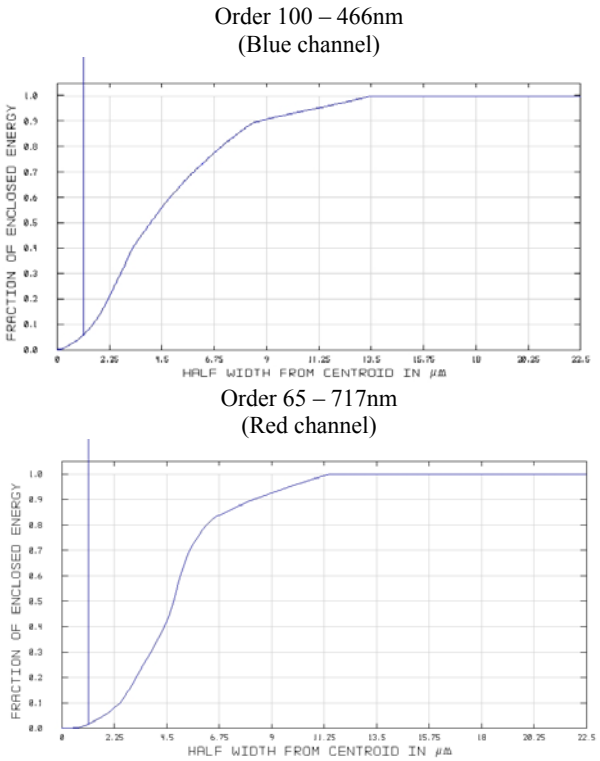

Figure 5. Ensquared energy plots.

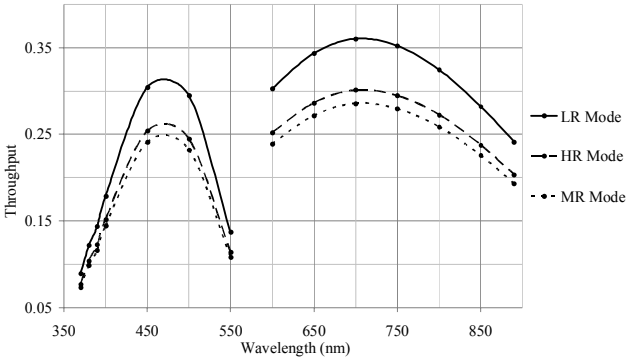

Figure 6. Comparison of throughput between spectrograph modes.

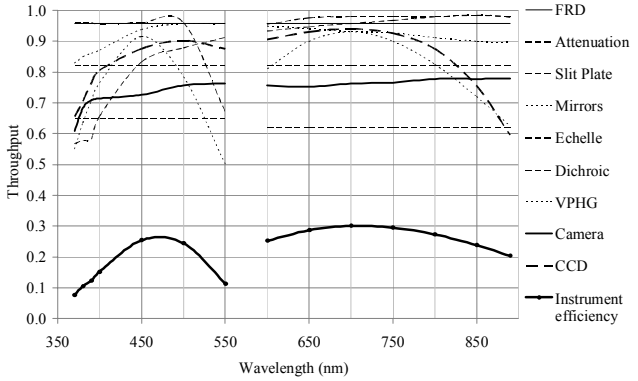

Figure 7. Throughput efficiency contributions by component.

case plots of the ensquared energies re-computed with the latest optical models, are shown for the central wavelength and central order (hence chip and field centre) in Figure 5. For the blue channel example shown, 95% of the ensquared energy is within a 25µm box. At these wavelengths 80% of the energy is within one 15µm pixel. In the red arm example shown more than 95% of the encircled energy within a box 25µm square up to 800nm. By order 53 (871nm) performance is degraded such that only 55% of the encircled energy within a box 25µm square.

2.4.2 Throughput

The manufacturing specifications for most of the optical elements have now been agreed upon and this has allowed a much more detailed throughput calculation to be done based on the specified materials and coatings to be used. The predicted efficiencies of the low, medium and high resolution spectrograph modes are plotted in Figure 6 and the component contributions for the high resolution mode are shown in Figure 7. The model will be refined again when the witness samples of optical coatings used on the mirrors and the AR coatings on the transmissive elements are measured. The VPHG efficiency peaks give rise to the characteristic bell shape of the curves for the red and blue channels and are responsible for the dip in throughput performance towards the crossover. The low resolution mode has the highest throughput, as expected. The sliced modes include losses due to the input optics train and geometrical losses at the slit. The higher QE of the red CCD gives the better throughput in the red channel. In all modes the extreme blue performance is limited by the attenuation of the optical fibres. Iodine cell and double scrambler losses in the high stability mode are likely to be considerable but are not yet quantified and so do not arrear in the figures.

3. IMPLEMENTATION

3.1 Manufacturing

At the time of writing in May 2010, manufacture of the instrument is well underway. The stainless steel vacuum tank has now been commissioned and is ready to accept the optical components. The manufacture of the optical supports has commenced. The optical mounts for the large reflective optics, including the échelle grating, take advantage of the prior art which has proven reliable in earlier spectrographs, most notably UVES[5], FEROS[6] and PEPSI[7], examples are given in Figure 8.

3.1.1 Échelle

The échelle grating is a mosaic replica that has been fabricated by Richardson Gratings. The grating has been optically tested and the results are summarized in Table 1. Efficiencies given in the table were measured using a spectrograph equipped with a movable camera, positioned to intercept the diffracted light at 130th, 117th, 85th and 52nd orders which correspond to the wavelengths listed. The values given in the table are the un-polarised (average S&P plane) efficiencies. The efficiency uniformity was also verified using an alternative setup. Interferometric measurements of surface figure were also taken in the form of three overlapping sub-aperture surface figure maps (each covering 150 x 600mm). When processed to remove the effect of piston, tilt and curvature, each sub aperture surface error is better than 0.3 waves. The Lyman ghosts remain essentially the same as the master grating from which the échelle was replicated.

3.2 Detectors

The e2v CCD 44-82 blue detector has now been integrated with the detector read out electronics by Astronomical Research Cameras, Inc., fully tested and characterised. The 2048 x 4096 chip (with 15µm pixels) has two readout registers and was tested in dual readout configuration. Table 2 summarizes the gain, readout noise and full well performance of the detector system at three readout speeds, 100kHz, 400kHz and 1MHz. The 400 kHz mode is likely to be the most commonly employed in HRS; reading out a full frame in approximately 40s. The 1MHz mode is a slight compromise between keeping readout noise within acceptable levels whilst maintaining full well performance, which is limited by the analogue to digital convertor (ADC). The CCD can also be used with pre-binning which, in addition to speeding up readout, increases full well capacity to approximately 220ke$^-$. In this regime the readout noise is high and is dominated by the ADC as considerably lower gain settings must be used to bring the CCD full well within the range of the ADC. Dark current has been measured at 2.15e$^-$/pixel/hour at -110˚C. The serial CTE was measured empirically to be 99.99897% at this temperature. It is not recommended that the CCD be operated at temperatures lower than this due to the deterioration in CTE.

The red CCD is a 4096 x 4112 e2v 231-84, again with 15µm pixels, and is currently under test. This chip is made from deep depletion silicon and has the Extra Red Plus fringe suppression option. The fringe suppression process attenuates the internal interference fringes seen at long wavelengths (>800nm) on thinned, backside illuminated CCDs as described by Jorden *et al*[8].

3.3 Enclosure

The optical layout of SALT HRS implies a physical size of approximately 4m x 1.3m. The instrument itself will be located in the spectrograph room below the SALT telescope and the optical fibres will be routed in a conduit from the telescope prime focus approximately 30m above. The whole spectrograph will be housed inside a vacuum tank (see Figure 9) in a temperature controlled environment for maximum stability. To attain temperature stability approaching 1mK on the optical bench, a two-stage temperature control scheme has been devised. An outer enclosure regulated by a close-control air conditioning unit operating at 20˚C provides immunity from seasonal variation and daily temperature

Parameter	Measurement
Spectral resolution	736, 000 at 632.8nm
Spatial resolution	~0.3 arc sec
Ghost intensity	< 4.0 x 10^{-5} (relative to parent)
Blaze angle	76.2˚
Efficiency	> 67% at 360nm > 65% at 400nm > 63% at 550nm > 62% near 900nm

Table 1 Summary of Measured Échelle Characteristics

	Left channel			Right channel		
Readout speed (kHz)	**Readout noise (e$^-$)**	**Conversion Gain (e$^-$/ADU)**	**Full well (ke$^-$)**	**Readout noise (e$^-$)**	**Conversion Gain (e$^-$/ADU)**	**Full well (ke$^-$)**
100	3.804	2.686	~160	3.627	2.778	~160
400	4.129	2.453	~150	4.291	2.506	~150
1000	5.786	1.829	~110	5.860	1.858	~110

Table 2 Summary of Blue CCD Performance Characterisation

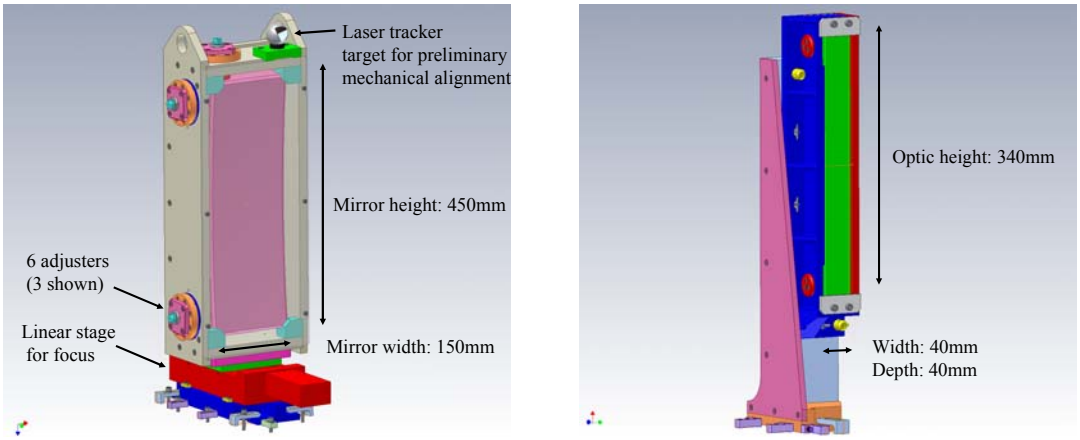

Figure 8. Examples of optics mounts: Pupil mirror (left) and dichroic (right).

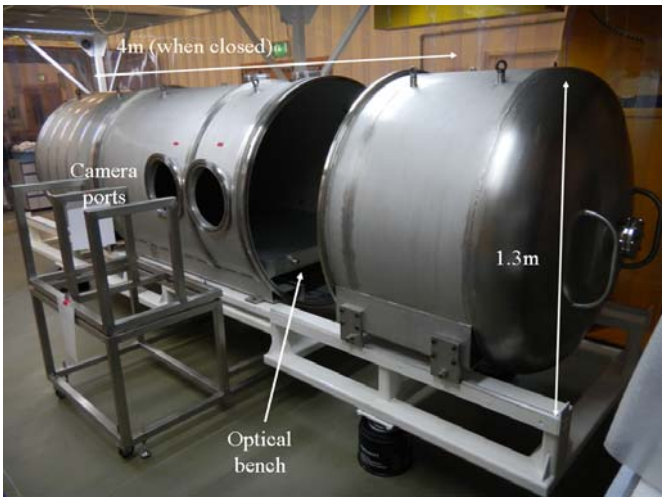

Figure 9. SALT HRS Vacuum Tank, 4 m long and 1.3 m in diameter. The rails upon which it sits allow the tank sections to be separated.

cycles. The instrument is further insulated by an isolation box inside which the vacuum vessel will be regulated to a slightly elevated temperature of 22˚C by a closed loop temperature controller, with heating being applied via heater pads or heating wire in direct contact with the vessel itself.

3.4 Hardware Control and Image Acquisition Software

All of the SALT HRS software will be LabView-based. The system will be distributed over several PCs with inter-process communication provided by standard middleware. The software is implemented as a series of layers. The control layer contains the application(s) that provide the user interface. The sequencer layer is the core of the control system. It interprets commands from the user interface and sequences them to the hardware via the server layer. The server layer is closely bound to the hardware with applications that run on the PC that contains the relevant control cards and their driver software. The server layer software will be highly abstracted from the sequencer layer software for ease of maintenance and to enable any future upgrades to be accomplished with minimal effort.

4. EXEMPLAR SCIENCE

The SALT HRS science case was developed through community consultation when the instrument was undergoing its early design phases. A number of scientific applications were identified which informed later design stages. Four (non-

exhaustive) categories of science and the constraints they place on the design and operation of the spectrograph are set out below.

4.1 Stellar radial velocity measurements

While errors as large as several km s^{-1} (or even larger) are often tolerable for radial velocity measurements of kinematically "hot" stellar populations or high-amplitude spectroscopic binary stars, studies of kinematically "cooler" populations or lower amplitude binaries have routinely achieved ~1 km s^{-1} accuracy. Many stellar studies could have benefitted from better than 1 km s^{-1} accuracy in order to detect binaries with low inclination or long orbital periods, for which dv_{rad}/dt is very low; 1 km s^{-1} is more a reflection of what was relatively readily achievable at échelle resolutions without high stability instruments or iodine cells. However, precision radial velocities measured using high stability spectrographs, in some cases with iodine cells, are approaching 0.5 m s^{-1} accuracy in the search for ever-lower mass planets around other stars. The SALT HRS vacuum enclosure (Sect. 3.3) avoids variations in the refractive index of air with pressure or temperature, which is one of the major limitations on accuracy at the sub-km s^{-1} level. The fibre-fed HARPS[9], an evacuated spectrograph on the ESO 3.6 m telescope, regularly attains 1 m s^{-1} accuracy (at R = 115000) without an iodine cell. SALT HRS will have to achieve comparable precision to be competitive in planet detection. SALT HRS will also provide data for kinematic and dynamical studies of faint stellar populations in the Galaxy (e.g. in the outer halo where accreted substructures are expected to be best preserved) and some Local Group targets.

4.2 Stellar atmosphere analysis

Stellar atmosphere analyses cover a wide range of scientific goals associated with the photospheres, chromospheres and coronae of stars at different stages of stellar evolution. Their scientific interest arises from the different stellar populations to which they belong, or because they exhibit a range of evolutionary phenomena as late-type active stars, pulsating stars, stars with winds, and interacting binaries. Such studies often require high resolution data of widely separated spectral features, a task for which cross-dispersed échelle spectrographs like SALT HRS are designed. Simultaneity at widely separated wavelengths is not only more efficient of observing time but can be crucial in the case of variable phenomena related to outbursts or orbital phase, and precludes the use of conventional spectrographs. This partially drove the requirement for blueward coverage (Figure 6) extending to the important chromospheric diagnostics of the Ca II 393 and 396 nm lines, as well as Balmer series lines. Doppler tomography and eclipse mapping are two examples of the unique outputs achievable from observations of this nature.

4.3 Chemical compositions of stars

Spectra used for detailed abundance analyses of individual stars are obtained at high S/N (30-200) and are usually photon-noise limited. For a given number of photons per nanometer, abundance studies generally benefit more from high spectral resolution than from high S/N in the continuum. This partially drove the requirement for the high resolving-power mode having R ~ 67000. High resolving powers are also essential for interpreting blended spectral features, and for elements which present only a few spectral lines, it may be unavoidable to work with partially blended features. Examples include the lines of minor-fraction isotopes (e,g, ^{6}Li) and important trace species (e.g. the neutron-capture elements, especially the radioactive nuclides Th and U). Regrettably, higher resolving powers usually require a reduction in throughput (Sect. 2.4.2), and hence the number of delivered photons per nanometre is not fixed. Not all stellar atmosphere analysis work requires or benefits from the highest resolutions; in particular work involving intrinsically broad lines such as those in rotating O and B stars. Chemical composition studies contribute to fields including the study of the stellar populations and chemical evolution of the Galaxy and nearby Local Group members (of which the SMC and LMC will be important SALT HRS targets). The Galactic population studies RAVE[10] (underway on the UK Schmidt telescope) and Gaia (data release after 2015) are based around the Ca IR triplet at 870 nm, as are many other population studies involving late-type giants. It is important to cover this region with SALT HRS since it is well characterised and has shown its value in other studies as one of the few red spectral regions with high data content for population studies. This partially drove the requirement for the red cutoff of SALT HRS (Figure 6).

4.4 Interstellar and intergalactic absorption

The low temperature of interstellar gas seen in absorption against background sources (stars and quasars) means that resolving powers of up to one million can be valuable. Clearly SALT HRS will not compete with work having those requirements. Nevertheless, it will be one of the largest telescopes capable of simultaneously recording widely separated absorption lines and diffuse interstellar bands at resolving power of R ~ 67000, and hence should make an important contribution to the study of Galactic, Local Group and high-redshift absorbers, particularly for faint sources which have

been out of the reach of more modest telescopes. It is anticipated that studies of interstellar chemistry at high redshift will grow rapidly over the next decade.

ACKNOWLEDGEMENTS

The authors would like to thank the many companies and individuals who have contributed to SALT HRS. We especially thank Richardson Gratings, Astronomical Research Cameras, Inc. and Asahi Spectra Co., Ltd. for giving permission to reproduce their test results.

REFERENCES

[1] Barnes, S. I. *et al*, "The optical design of the Southern African Large Telescope High Resolution Spectrograph: SALT HRS," Proc. SPIE, 7014, 70140K, (2008).
[2] Loewen, E. G. and Popov, E., [Diffraction Gratings and Applications], Marcel Dekker Inc., (1997)
[3] Glazebrook, K. and Bland-Hawthorn, J., "Microslit Nod-Shuffle Spectroscopy: A Technique for Achieving Very High Densities of Spectra," Publications of the Astronomical Society of the Pacific, 113, 197–214 (2001).
[4] Schmoll, J., Roth, M. M. and Laux, U., "Statistical Test of Optical Fibre for Use in PMAS, the Potsdam Multi-Aperture Spectrophotometer," PASP, 115, 854-868 (2003).
[5] "http://www.eso.org/sci/facilities/paranal/instruments/uves/"
[6] "http://www.eso.org/lasilla/instruments/feros/"
[7] "http://www.aip.de/pepsi/ "
[8] Jorden, P. R., Pool, P. and Holtom R., "Latest EEV CCD developments, and technologies for scientific CCDs," Proceedings of 1999 ESO CCD Workshop, September 1999 Optical Detectors for Astronomy II, Kluwer Academic Publishers, (2000).
[9] "http://www.eso.org/sci/facilities/lasilla/instruments/harps/"
[10] "http://www.rave-survey.aip.de/rave/"